Qubit Noise Spectroscopy for Non-Gaussian Dephasing Environments

Leigh M. Norris, Gerardo A. Paz-Silva, and Lorenza Viola

Phys. Rev. Lett. **116**, 150503 — Published 14 April 2016

DOI: 10.1103/PhysRevLett.116.150503

Qubit noise spectroscopy for non-Gaussian dephasing environments

Leigh M. Norris,[1] Gerardo A. Paz-Silva,[2] and Lorenza Viola[1]

[1] *Department of Physics and Astronomy, Dartmouth College, 6127 Wilder Laboratory, Hanover, New Hampshire 03755, USA*
[2] *Centre for Quantum Dynamics & Centre for Quantum Computation and Communication Technology, Griffith University, Brisbane, Queensland 4111, Australia*

(Dated: April 1, 2016)

We introduce open-loop quantum control protocols for characterizing the spectral properties of non-Gaussian noise, applicable to both classical and quantum dephasing environments. By engineering a multi-dimensional frequency comb via repetition of suitably designed pulse sequences, the desired high-order spectra may be related to observable properties of the qubit probe. We prove that access to a high time resolution is key to achieve spectral reconstruction over an extended bandwidth, overcoming limitations of existing schemes. Non-Gaussian spectroscopy is demonstrated for a classical noise model describing quadratic dephasing at an optimal point, as well as a quantum spin-boson model out of equilibrium. In both cases, we obtain spectral reconstructions that accurately predict the qubit dynamics in the non-Gaussian regime.

PACS numbers: 03.67.Pp, 03.65.Yz, 03.67.Lx, 07.05.Dz

Accurately characterizing the spectral properties of environmental noise in open quantum systems has broad practical and fundamental significance. Within quantum information processing, this is a prerequisite for optimally tailoring the design of quantum control and error-correcting strategies to the noisy environment that qubits experience, and for testing key assumptions in fault-tolerance threshold derivations [1]. From a physical standpoint, precise knowledge of the noise is necessary for quantitatively modeling and understanding open-system dynamics, with implications ranging from the classical-to-quantum transition to non-equilibrium quantum statistical mechanics and quantum-limited metrology [2].

Quantum noise spectroscopy seeks to characterize the spectral properties of environmental noise by using a controlled quantum system (a qubit under multi-pulse control in the simplest case) as a dynamical probe [3]. In recent years, interest in quantum noise spectroscopy has heightened thanks to both improved theoretical understanding of open-loop controlled dynamics in terms of transfer filter-function (FF) techniques [4, 5] and experimental validation in different qubit platforms. In particular, quantum control protocols based on dynamical decoupling (DD) have been successfully implemented to characterize noise properties during memory and driven evolution in systems as diverse as solid-state nuclear magnetic resonance [6], trapped ions [7], superconducting [8] and spin [9] qubits, and nitrogen vacancy centers in diamond [10].

Despite the above advances, existing noise spectroscopy protocols suffer from several disadvantages. Notably, they are restricted to *classical, Gaussian* phase noise. While dephasing (T_2-) processes are known to provide the dominant decoherence mechanism in a variety of realistic scenarios, the Gaussianity assumption is *a priori* far less justified. On the one hand, the Gaussian approximation typically breaks down in situations where the system is strongly coupled to a sparse environment – such as discrete frequency modes [7], or bistable fluctuators responsible for $1/f$ noise, as ubiquitously encountered in solid-state nanodevices [11]. Even for environments well described by a continuum of modes, non-Gaussian noise statistics may be generally expected away from thermal equilibrium, or whenever symmetry considerations forbid a linear coupling [12]. In all such cases, accurate noise spectroscopy mandates going beyond the Gaussian regime.

In this paper, we introduce open-loop control protocols for characterizing *stationary, non-Gaussian dephasing* using a qubit probe. Our approach is applicable to classical noise environments and to a paradigmatic class of open quantum systems described by linearly coupled oscillator environments – as long as all noise spectra are sufficiently smooth. While we build on noise spectroscopy by sequence repetition as proposed by Alvarez and Suter [6], our central insight is to leverage the structure of FFs in the dephasing setting to establish the emergence of a frequency comb for arbitrary high-order noise spectra (so-called $polyspectra$), paving the way to the desired multi-dimensional spectral estimation. We first demonstrate the power of our approach for Gaussian noise, where we extend the range of spectral reconstruction over existing protocols. For non-Gaussian noise, we reconstruct the spectra associated with the leading high-order cumulants, absent in the Gaussian limit. Quantitative prediction of the qubit's free evolution in the presence of these non-Gaussian environments reveals how, in both the classical and quantum case, polyspectra are essential to capture additional dynamical contributions unaccounted for in the Gaussian regime.

Control setting and noise polyspectra.– We consider a qubit S coupled to an uncontrollable environment (bath) B. In the interaction picture with respect to the bath Hamiltonian, H_B, and the qubit Hamiltonian, $H_S = \hbar\omega_0\sigma_z/2$, the joint system is described by $H(t) = \hbar\sigma_z B(t)/2 + H_{\text{ctrl}}(t)$, where the first term accounts for the bath-induced dephasing and $H_{\text{ctrl}}(t)$ is the external open-loop control, acting non-trivially on the qubit alone. For a classical bath, $B(t)$ is a stochastic process, whereas $B(t)$ is a time-dependent operator for a quantum bath. The applied control consists of repeated sequences of π-pulses (say, about x), which for simplicity we take to be instantaneous. After transforming to the interaction picture associated with $H_{\text{ctrl}}(t)$, the joint Hamiltonian becomes

$\tilde{H}(t) = y(t)\hbar\sigma_z B(t)/2$, where the "switching function" $y(t)$ toggles between ± 1 with every π-pulse applied to the qubit.

The effect of dephasing is seen in the dynamics of the qubit's coherence element, which we may express in terms of bath-operator cumulants. Specifically, $\langle\sigma_+(t)\rangle = \langle\sigma_+(0)\rangle\, \mathrm{e}^{-\chi(t)+i\phi(t)}$, where the decay parameter and phase angle are respectively given by:

$$\chi(t) = \sum_{\ell=1}^{\infty} \frac{(-1)^\ell}{(2\ell)!}\Upsilon^{(2\ell)}(t),\ \phi(t) = \sum_{\ell=1}^{\infty} \frac{(-1)^\ell}{(2\ell+1)!}\Upsilon^{(2\ell+1)}(t),$$
$$\Upsilon^{(k)}(t) \equiv \int_0^t dt_1 \ldots \int_0^t dt_k\, y(t_1)\ldots y(t_k) C^{(k)}(t_1,\ldots,t_k).$$

The kth-order cumulant $C^{(k)}(t_1,\ldots,t_k)$ depends on the bath correlation functions $\langle B(t_1)\ldots B(t_j)\rangle$, $j \le k$, and $\langle\,\cdot\,\rangle$ denotes a classical ensemble average or an expectation value with respect to the initial bath state, $\rho_B(0)$, in the quantum case. For zero-mean Gaussian noise, $C^{(k)}(t_1,\ldots,t_k) \equiv 0$ except for $k=2$. Thus, Gaussian noise gives *no phase evolution*. For non-Gaussian noise, higher-order even (odd) cumulants contribute to decay (phase evolution), respectively.

For stationary noise, where $C^{(n+1)}(t_1,\ldots,t_{n+1})$ is a function of the time separations $\tau_j \equiv t_{j+1}-t_1$, $j\in\{1,\ldots,n\}$, the noise spectral properties are fully characterized by the Fourier transforms of the cumulants with respect to $\{\tau_j\}$. Letting $\vec{v}_n \equiv (v_1,\ldots,v_n)$, the *nth-order polyspectrum* is

$$S_n(\vec{\omega}_n) \equiv \int_{\mathbb{R}^n} d\vec{\tau}_n\, e^{-i\vec{\omega}_n\cdot\vec{\tau}_n} C^{(n+1)}(\vec{\tau}_n), \quad n\ge 1, \tag{1}$$

where $S_1(\vec{\omega}_1) \equiv S(\omega)$ is the familiar power spectral density (PSD), and $S_2(\vec{\omega}_2)$ and $S_3(\vec{\omega}_3)$ are known as the "bi-spectrum" and "tri-spectrum". For all orders, $S_n(\vec{\omega}_n)$ is a smooth n-dimensional surface when the noise is classical and ergodic [13]. In general, $C^{(n+1)}(t_1,\ldots t_{n+1})$ may depend on fewer than n time separations, leading to the presence of delta functions in $S_n(\vec{\omega}_n)$. All polyspectra possess a high degree of symmetry, *irrespective of the noise*. That is, $S_n(\vec{\omega}_n)$ is fully specified in all frequency space by its value on a particular subspace, $\mathcal{D}_n$, known as the *principal domain* [14].

Noise spectroscopy protocol.– Our objective is to characterize not only the PSD but the polyspectra. We accomplish this by generalizing the DD noise spectroscopy protocol proposed in [6] for Gaussian noise. This protocol relies on repetitions of identical *base sequences*, whose duration ("cycle time") we shall denote by T. Following [5], the effect of a base control sequence p in the frequency domain is characterized by a single *fundamental FF*, $F_p(\omega) \equiv \int_0^T dt e^{+i\omega t} y_p(t)$. If $|\vec{\omega}_{k-1}| \equiv \omega_1 + \ldots + \omega_{k-1}$, direct calculation shows that M repetitions of p yield

$$\Upsilon^{(k)}_{[p]^M} = \int_{\mathbb{R}^{k-1}} d\vec{\omega}_{k-1} \prod_{j=1}^{k-1} F_p(\omega_j) \frac{\sin(M\omega_j T/2)}{\sin(\omega_j T/2)} \times F_p(-|\vec{\omega}_{k-1}|) \frac{\sin(M|\vec{\omega}_{k-1}|T/2)}{\sin(|\vec{\omega}_{k-1}|T/2)} \frac{S_{k-1}(\vec{\omega}_{k-1})}{(2\pi)^{k-1}}, \tag{2}$$

The key to extending the protocol in [6] beyond Gaussian noise ($k=2$) is to realize that *repetition produces a multi-dimensional frequency comb for all orders*, namely,

$$\prod_{j=1}^{k-1}\Big[\frac{\sin(M\omega_j T/2)}{\sin(\omega_j T/2)}\Big] \frac{\sin(M|\vec{\omega}_{k-1}|T/2)}{\sin(|\vec{\omega}_{k-1}|T/2)} \approx M \prod_{j=1}^{k-1}\Big[\frac{2\pi}{T}\sum_{n_j=-\infty}^{\infty}\delta\Big(\omega_j - \frac{2\pi n_j}{T}\Big)\Big], \quad M\gg 1, \forall k, \tag{3}$$

provided that $S_{k-1}(\vec{\omega}_{k-1})$ in Eq. (2) is a smooth function.

Thanks to the "hyper-comb" in Eq. (3), obtaining the polyspectra becomes an inverse problem. Substituting Eq. (3) into Eq. (2) produces a linear equation that couples the polyspectra and the FFs evaluated at the harmonic frequencies $\mathcal{H}_j \equiv \{2\pi\vec{n}_j/T \,|\, \vec{n}_j \in \mathbb{Z}^j\}$,

$$\Upsilon^{(k)}_{[p]^M} = \sum_{\vec{h}_{k-1}\in\mathcal{H}_{k-1}} \frac{M}{T^{k-1}} \prod_{j=1}^{k-1} F_p(h_j) F_p(-|\vec{h}_{k-1}|) S_{k-1}(\vec{h}_{k-1}). \tag{4}$$

To obtain a finite linear equation, we need to truncate the above sum to a finite set Ω_{k-1}. With no prior knowledge of the noise, it suffices to consider $\Omega_{k-1} \subset \mathcal{D}_{k-1}\cap\mathcal{H}_{k-1}$ in the principal domain of the polyspectrum. Using the truncated expression in Eq. (4) enables us to relate the sampled polyspectra to experimentally observable dynamical quantities, that is

$$\chi_{[p]^M} \approx \sum_{\ell=1}^{\infty} \frac{(-1)^\ell M}{(2\ell)!\, T^{2\ell-1}} \sum_{\vec{h}_{2\ell-1}\in\Omega_{2\ell-1}} m_{2\ell-1}(\vec{h}_{2\ell-1}) \times \prod_{j=1}^{2\ell-1} F_p(h_j) F_p(-|\vec{h}_{2\ell-1}|) S_{2\ell-1}(\vec{h}_{2\ell-1}), \tag{5}$$

$$\phi_{[p]^M} \approx \sum_{\ell=1}^{\infty} \frac{(-1)^\ell M}{(2\ell+1)!\, T^{2\ell}} \sum_{\vec{h}_{2\ell}\in\Omega_{2\ell}} m_{2\ell}(\vec{h}_{2\ell}) \times \prod_{j=1}^{2\ell} F_p(h_j) F_p(-|\vec{h}_{2\ell}|) S_{2\ell}(\vec{h}_{2\ell}), \tag{6}$$

where the multiplicity $m_n(\vec{h}_n) \equiv \mathrm{card}\{\vec{h}_n \in \mathbb{R}^n \,|\, S_n(\vec{h}_n) = S_n(\vec{\omega}_n),\ \forall\omega_n \in \mathcal{D}_n\}$ accounts for the symmetry of the polyspectrum. When contributions from high-order correlation functions are negligible (e.g., for sufficiently small time and/or noise strength), the cumulant expansion in Eqs. (5)-(6) may be truncated at $\ell = L$. If N terms are retained, measuring $\chi_{[p]^M}$ ($\phi_{[p]^M}$) for at least N control sequences creates a system of linear equations, that can be inverted to obtain the odd (even) polyspectra up to order $2L-1$ ($2L$) [15].

Base sequence construction.– In the noise spectroscopy protocol of [6], a *fixed* base sequence is used (CPMG, after Carr, Purcell, Meiboom, and Gill), with cycle times varying from T to $T/n = 2\tau$, where $n\in\mathbb{Z}^+$ and τ is the minimum time between pulses. While this produces a well-conditioned linear inversion, both the number of distinct control sequences

and the range of spectral reconstruction are limited – in particular, $|\omega| \leq \pi/\tau$ for a minimum allowed $\tau > 0$. The use of a fixed DD sequence has an additional disadvantage: CPMG refocuses static noise ($F_{\text{cpmg}}(\omega = 0) = 0$, hence the "filtering order" is non-zero [5]), precluding reconstruction at any point in frequency space containing a zero, a substantial information loss for higher-dimensional polyspectra.

Non-Gaussian noise spectroscopy demands a *large number of sequences with spectrally distinct FFs*, including some with zero filtering order. We generate a family of base sequences satisfying these requirements by using different orders of concatenated DD, CDD$_m$: namely, not only CPMG ($m = 2$), but also durations of free evolution ($m = 0$), up to $m = 5$. The presence of free evolution permits sequences with zero filtering order, enabling the polyspectra to be reconstructed at points containing a zero. Specifically, let a *fixed* cycle time T be expressed in terms of a minimum *time resolution* δ, $T \equiv q\delta$, where $q \in \mathbb{Z}^+$. While all pulse times will be integer multiples of δ, δ and τ are two independent constraints a priori, with $\delta < \tau$ typically. If $q \equiv \sum_i q_i$ is an integer partition of q, we place a CDD$_m$ sequence into the ith interval, of duration $q_i\delta$, subject to the condition that no two pulses are separated by less than τ. As shown in the Supplement [16], the range of spectral reconstruction is bounded by $|\omega| \leq \pi/\delta$. A high resolution (small δ) is key to generate sequences with *incommensurate* periodicities, making it possible to achieve spectral reconstruction over an extended range.

The added capabilities of our control sequences may be appreciated already for spectroscopy of classical Gaussian noise, see Fig. 1. In this case, Eq. (5) truncates exactly at $\ell = 1$; this produces a system of linear equations relating the desired PSD to $\chi_{[p]^M}$, which we obtain numerically for each control sequence. In addition to accurately reconstructing the larger peaks over the expanded range $|\omega| \leq 48\pi/T = 3\pi/\tau$, our protocol successfully resolves the small peak at $\omega = 0$, thanks to inclusion of control sequences with zero filtering order.

Non-Gaussian spectral reconstructions.– We now return to our main goal, namely characterizing non-Gaussian polyspectra. As a first example, we consider a classical "square noise" process arising from a quadratic coupling to a Gaussian source, as encountered in superconducting qubits operating at an optimal working point [11, 17]. That is, $B(t) \equiv \xi_a(t) = a\big(g(t)^2 - \langle g(t)^2\rangle\big) + \big(1-a\big)g(t)$, where $g(t)$ is a zero-mean Gaussian process, and $a \in [0,1]$ interpolates between Gaussian ($a = 0$) and fully non-Gaussian ($a = 1$) regimes. Truncating Eq. (6) at the leading $\ell = 1$ term allows us to reconstruct the bi-spectrum $S_2(\vec{\omega}_2)$ from numerically determined values of $\phi_{[p]^M}$. Here, the relevant principal domain $\mathcal{D}_2$ is an octant bounded by $\omega_1 = \omega_2$ and $\omega_1 = 0$. Reconstructing 35 points in $\mathcal{D}_2$ enables us to obtain $S_2(\vec{\omega}_2)$ at 325 points in $\mathbb{R}^2$. Representative results for the actual vs. reconstructed bi-spectrum at $a = 1$ are shown in Fig. 2(a)-(b). The relative error in 2(c) indicates very good agreement at the interior points, but larger error in the tails. Because there is minimal spectral concentration in the tails, however, this error has little effect on the qubit dynamics. As Fig. 3 shows, excellent agreement is found between the theoretical phase evolution and the one predicted by the reconstructed bi-spectrum.

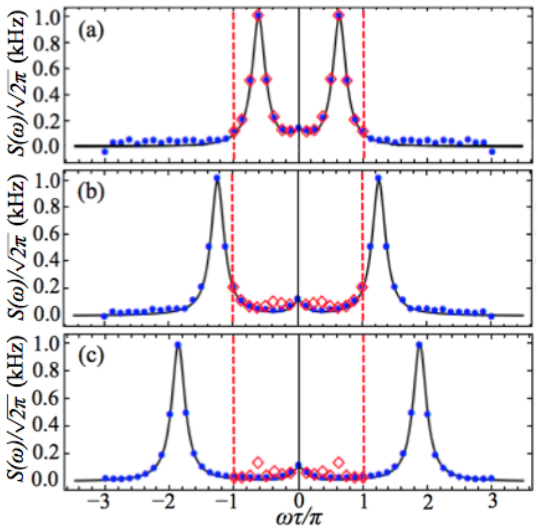

FIG. 1. (Color online) Comparison between Alvarez-Suter's (red diamonds) and our protocol (blue dots) in reconstructing a Gaussian PSD (black solid line) with increasing high-frequency components (top to bottom). Both protocols use $M = 50$ repetitions of sequences with $\tau = 3.1\times10^{-4}$ s and $T = 16\tau$. For our protocol, we employ 25 base sequences assembled from CDD$_m$, $m = 0,\ldots,4$. The PSD is a sum of Lorentzian peaks, $S(\omega) = w_1/[1 + (8\omega/\omega_c)]^2 + w_2/\{1 + [8\,(\text{sign}(\omega)\omega - d)/\omega_c)^2]\}$, where $w_1/\sqrt{2\pi} = 0.1$ kHz, $w_2/\sqrt{2\pi} = 1$ kHz, $\omega_c = 10$ kHz $\approx \pi/\tau$, and d controls the offset of the high-frequency peaks, $d = \frac{5}{8}\pi/\tau$ (a), $d = \frac{10}{8}\pi/\tau$ (b), $d = \frac{15}{8}\pi/\tau$ (c). As the original protocol can only reconstruct $S(\omega)$ up to $|\omega| < \pi/\tau$ (dashed vertical lines), it cannot "see" the high-frequency peaks in (b)-(c), which results in instability at lower frequencies.

Extending noise spectroscopy to quantum environments entails qualitatively new challenges because non-Gaussian statistics ensues from the *combined effect of the bath operators $B(t)$ and the initial bath state $\rho_B(0)$*, and no general characterization of quantum polyspectra (and their smoothness properties) is available to our knowledge. We take a first step in this direction by focusing on linearly coupled spin-boson environments, whereby $H_B = \hbar\sum_k \Omega_k a_k^\dagger a_k$ and $B(t) = \sum_k (g_k e^{i\Omega_k t}a_k^\dagger + \text{h.c.})$, with $a_k, a_k^\dagger$ being canonical bosonic operators and Ω_k, g_k having units of (angular) frequency. For a general quantum bath, the noise is stationary if and only if $[H_B, \rho_B(0)] = 0$. This prevents non-zero odd cumulants, hence the qubit undergoes no phase evolution.

Given any stationary, non-Gaussian bath state $\rho_B(0)$ we can reconstruct spectral quantities associated with the first two leading-order even cumulants, $S(\omega)$ and $S_3(\vec{\omega}_3)$. Although $S(\omega)$ is *asymmetric* about $\omega = 0$, the fact that arbitrary FFs enter through even combinations implies that we can only reconstruct an "effective spectrum", $S_{\text{eff}}(\omega) \equiv [S(\omega) + S(-\omega)]/2$, as relevant to the qubit dephasing dynamics. As shown in [16], the tri-spectrum for any *non-separable*, stationary initial bath state has the form $S_3(\vec{\omega}_3) = (2\pi)^3[\delta(\omega_1+\omega_2)J_3(\omega_1,\omega_3) + \delta(\omega_2+\omega_3)J_3(\omega_1,\omega_2) + \delta(\omega_1+$

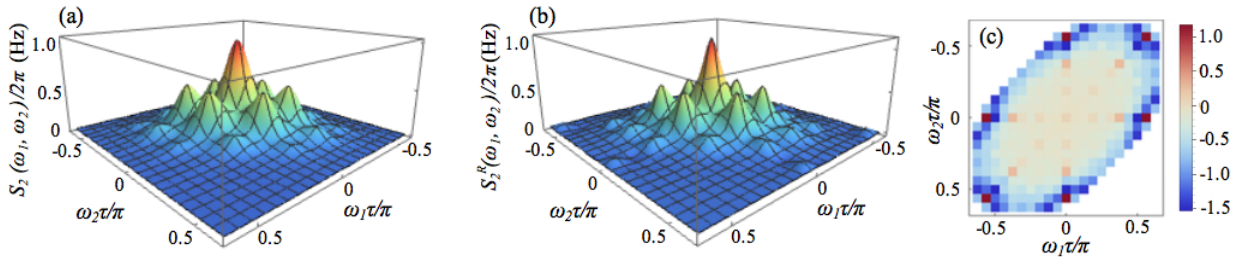

FIG. 2. (Color online) Actual bispectrum, $S_2(\vec{\omega}_2)$ (a), vs. reconstructed bispectrum, $S_2^R(\vec{\omega}_2)$ (b), and relative error $E(\vec{\omega}_2) \equiv [S_2^R(\vec{\omega}_2) - S_2(\vec{\omega}_2)]/S_2(\vec{\omega}_2)$ (c), for classical non-Gaussian square noise $\xi_1(t) = g(t)^2 - \langle g(t)^2 \rangle$. Here, $g(t)$ is Gaussian with spectrum $S_g(\omega) = w_1/[1+8(\omega/\omega_c)^2] + w_2/[1+16\,(\mathrm{sign}(\omega)\omega/\omega_c - 3/2)^2]$, and $w_1 = 1/10$ Hz, $w_2 = 1/25$ Hz. The protocol uses $M = 40$ repetitions of sequences composed of CDD_{0-5}, with $\tau = 3.95\times10^{-5}$ s and $T = 32\tau$ to reconstruct the bi-spectrum at 325 points. Grid lines in (a) and (b) are drawn at harmonic frequencies. In (b), these values have been smoothed with a spline interpolation. The largest relative errors occur in the high-frequency regions at the outer edge of the bi-spectrum which, however, contribute far less to the qubit dynamics.

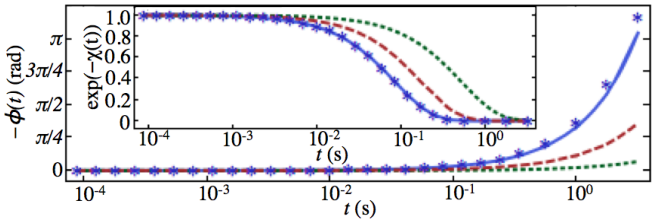

FIG. 3. (Color online) Phase evolution and decay (inset) of a qubit under square noise $\xi_a(t)$ with different degrees of Gaussianity [see text], and same spectrum $S_g(\omega)$ for $g(t)$ as in Fig. 2. Curves are ordered according to decreasing non-Gaussianity: $a = 1$ (blue solid), $a = 0.7$ (red dashes) and $a = 0.4$ (green dots). For the fully non-Gaussian $a = 1$ case, we used the reconstructed spectrum and bi-spectrum [Fig. 2] to predict the qubit decay and phase evolution (blue asterisks), showing excellent agreement with the theoretical evolution, computed up to the fifth-order cumulant.

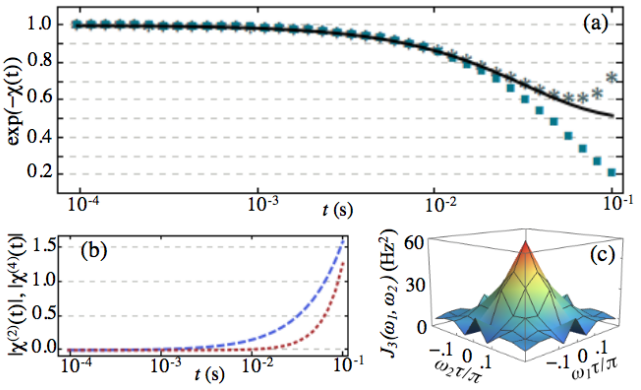

FIG. 4. (Color online) Qubit decay under non-Gaussian spin-boson dephasing (a), relative strengths of the first two terms in the cumulant expansion for $\chi(t)$ (b), reconstructed effective tri-spectrum (c), with grid lines at harmonic frequencies. The non-Gaussian bath state $\rho_B(0) = \rho_{T_1}/2 + \rho_{T_2}/2$, where ρ_{T_1}, ρ_{T_2} are thermal states at temperatures $T_1 = 7.64$K, $T_2 = 7.64\times10^3$K. Ohmic spectral density $J(\omega) = w_0|\omega/\omega_c|e^{-(\omega/\omega_c)^2}$ is assumed, with $w_0 = 0.1$ nHz, $\omega_c = 10$ kHz. The curves in (a) represent theoretical decay (black solid), decay predicted by reconstructing $S_{\mathrm{eff}}(\omega)$ and $J_3(\omega_1,\omega_2)$ (grey asterisks), and decay predicted by reconstructing $S_{\mathrm{eff}}(\omega)$ only (Gaussian approximation, teal squares). The non-Gaussian prediction fails when $|\chi^{(4)}(t)|$ (red dashes) and $|\chi^{(2)}(t)|$ (blue dashes) in (b) become comparable. All reconstructions used $M = 50$ repetitions of 21 base sequences composed of CDD_{0-5}, with $\tau = 3.44\times10^{-5}$ s, $T = 32\tau$.

$\omega_3)J_3(\omega_2,\omega_3)]$. Because the hypercomb approximation holds only if $S_3(\vec{\omega}_3)$ is smooth, we cannot directly reconstruct it. We can, however, reconstruct the "effective tri-spectrum" $J_3(\vec{\omega}_2)$, provided it is smooth. Due to the delta functions in $S_3(\vec{\omega}_3)$, the terms in Eq. (5) associated with the tri-spectrum differ by a constant factor in the spin-boson case. The appropriate modified equations are derived in [16], along with similar equations for *separable* stationary initial states. In the absence of prior information about $\rho_B(0)$, comparison between predictions based on the two resulting reconstructions will enable the correct effective tri-spectrum to be inferred.

For illustration, we choose $\rho_B(0)$ to be a non-Gaussian, non-separable state corresponding to far-from-equilibrium conditions, and simultaneously reconstruct $S_{\mathrm{eff}}(\omega)$ and $J_3(\omega_1,\omega_2)$ by numerically determining $\chi_{[p]^M}$ and inverting the appropriate system of linear equations [16]. To test the accuracy of our reconstructions, we again predict the dynamics of the qubit under free evolution. As shown in Fig. 4(a), taking into account the non-Gaussianity of the noise by reconstructing both the effective spectrum and tri-spectrum improves the prediction by almost an order of magnitude in time. Because our non-Gaussian prediction uses only spectral quantities associated with the second and fourth cumulants, however, it fails when the latter becomes comparable in size to the second, indicating that the higher-order cumulants can no longer be neglected (see also Fig. 4(b)).

Conclusion.– We introduced control protocols for characterizing the high-order spectra associated with non-Gaussian dephasing on a qubit coupled to a classical or quantum bosonic environment. Our approach overcomes limitations of existing protocols, also allowing for spectral reconstruction over an extended bandwidth, which is of independent interest for quantum sensing applications. Our work points to the need for a deeper understanding of high-order quantum noise spec-

tra – including more complex dephasing settings described by non-linear spin-boson models or spin baths. We expect experimental implementation of our protocols to be within reach for various device technologies, in particular transmon or flux qubits [8], where a complete spectral characterization including high-order effects may be crucial for validating physical noise assumptions and discriminating between different microscopic theories of the noise itself [11, 18].

We thank M. Biercuk, W. Oliver, S. Gustavsson, and F. Yan for valuable discussions. Work at Dartmouth was supported from the US ARO under contract No. W911NF-14-1-0682 and the Constance and Walter Burke Special Projects Fund in Quantum Information Science. GAPS acknowledges support from the ARC Centre of Excellence grant No. CE110001027.

[1] J. Preskill, Quantum Inf. Comput. **13**, 181 (2013).

[2] H.-P. Breuer and F. Petruccione, *The Theory of Open Quantum Systems* (Oxford University Press, Oxford, 2002).

[3] R. J. Schoelkopf and A. A. Clerk and S. M. Girvin and K. W. Lehnert and M. H. Devoret, in *Quantum Noise in Mesoscopic Physics*, NATO Science Series **97**, 173 (2003); L. Faoro and L. Viola, Phys. Rev. Lett. **92**, 117905 (2004); T. Yuge, S. Sasaki, and Y. Hirayama, *ibid.* **107**, 170504 (2011); K. C. Young and K. B. Whaley, Phys. Rev. A **86**, 012314 (2012).

[4] T. J. Green, H. Uys, and M. J. Biercuk, Phys. Rev. Lett. **109**, 020501 (2012); A. Soare, H. Ball, D. Hayes, J. Sastrawan, M. C. Jarratt, J. J. McLoughlin, X. Zhen, T. J. Green, and M. J. Biercuk, Nature Phys. **10**, 825 (2014).

[5] G. A. Paz-Silva and L. Viola, Phys. Rev. Lett. **113**, 250501 (2014).

[6] G. A. Álvarez and D. Suter, Phys. Rev. Lett. **107**, 230501 (2011).

[7] S. Kotler, N. Akerman, Y. Glickman, and R. Ozeri, Phys. Rev. Lett. **110**, 110503 (2013).

[8] J. Bylander, S. Gustavsson, F. Yan, F. Yoshihara, K. Harrabi, G. Fitch, D. G. Cory, Y. Nakamura, J.-S. Tsai, and W. D. Oliver, Nature Phys. **7**, 565 (2011); F. Yan, S. Gustavsson, J. Bylander, X. Jin, F. Yoshihara, D. G. Cory, Y. Nakamura, T. P. Orlando, and W. D. Oliver, Nature Commun. **4**, 2337 (2013); F. Yoshihara, Y. Nakamura, F. Yan, S. Gustavsson, J. Bylander, W. D. Oliver, and J.-S. Tsai Phys. Rev. B **89**, 020503 (2014).

[9] O. Dial, M. D. Shulman, S. P. Harvey, H. Bluhm, V. Umansky, and A. Yacoby, Phys. Rev. Lett. **110**, 146804 (2013); J. T. Muhonen, J. P. Dehollain, A. Laucht, F. E. Hudson, T. Sekiguchi, K. M. Itoh, D. N. Jamieson, J. C. McCallum, A. S. Dzurak, and A. Morello, Nature Nanotech. **9**, 986 (2014).

[10] C. A. Meriles, L. Jiang, G. Goldstein, J. S. Hodges, J. Maze, M. D. Lukin, and P. Cappellaro, J. Chem. Phys. **133**, 124105 (2010); Y. Romach, C. Muller, T. Unden, L. J. Rogers, T. Isoda, K. M. Itoh, M. Markham, A. Stacey, J. Meijer, S. Pezzagna, B. Naydenov, L. P. McGuinness, N. Bar-Gill, and F. Jelezko, Phys. Rev. Lett. **114**, 017601 (2015).

[11] Y. M. Galperin, B. L. Altshuler, J. Bergli, D. Shantsev, and V. Vinokur, Phys. Rev. B **76**, 064531 (2007); E. Paladino, Y. M. Galperin, G. Falci, and B. L. Altshuler, Rev. Mod. Phys. **86**, 361 (2014).

[12] C. Uchiyama and M. Aihara, Phys. Rev. A **66**, 032313 (2002); M. F. Maghrebi, M. Krüger, and M. Kardar, arXiv:1508.00582.

[13] P. Guttorp and D. Brillinger, in *Selected Works of David Brillinger* (Springer New York, 2012) p. 149.

[14] V. Chandran and S. Elgar, IEEE Trans. Signal Proc. **42**, 229 (1994).

[15] This inverse problem can be solved by a variety of numerical methods. To assess the performance of the protocol with minimal computational resources, the simulations presented here utilize direct matrix inversion.

[16] See Supplemental Material at http://link.aps.org/xxx for additional technical details on spectral bandwidth enhancement and spectroscopy of bosonic noise.

[17] L. Cywiński, Phys. Rev. A **90**, 042307 (2014).

[18] J. Burnett, L. Faoro, I. Wisby, V. L. Gurtovoi, A. V. Chernykh, G. M. Mikhailov, V. A. Tulin, R. Shaikhaidarov, V. Antonov, P. J. Meeson, A. Ya. Tzalenchuk, T. Lindström, Nature Commun. **5**, 4119 (2014); J. Lisenfeld, G. J. Grabovskij, C. Müller, J. H. Cole, G. Weiss, and A. V. Ustinov, *ibid.* **6**, 6182 (2015).